Available online at www.sciencedirect.com
SCIENCE DIRECT®
Lithos 71 (2003) 505–527
LITHOS
www.elsevier.com/locate/lithos

The electrical structure of the Slave craton

Alan G. Jones[a,*,1], Pamela Lezaeta[b], Ian J. Ferguson[c], Alan D. Chave[b], Rob L. Evans[d], Xavier Garcia[a,b], Jessica Spratt[a,1]

[a] *Geological Survey of Canada, National Resources Canada, 615 Booth Street, Room 218, Ottawa, Ontario, Canada K1A 0E9*
[b] *Deep Submergence Laboratory, Department of Applied Ocean Physics and Engineering, Woods Hole Oceanographic Institution, Woods Hole, MA 02543, USA*
[c] *Department of Geological Sciences, University of Manitoba, Winnipeg, Manitoba, Canada R3T 2N2*
[d] *Department of Geology and Geophysics, Woods Hole Oceanographic Institution, Woods Hole, MA 02543, USA*

Abstract

The Slave craton in northwestern Canada, a relatively small Archean craton (600 × 400 km), is ideal as a natural laboratory for investigating the formation and evolution of Mesoarchean and Neoarchean sub-continental lithospheric mantle (SCLM). Excellent outcrop and the discovery of economic diamondiferous kimberlite pipes in the centre of the craton during the early 1990s have led to an unparalleled amount of geoscientific information becoming available.

Over the last 5 years deep-probing electromagnetic surveys were conducted on the Slave, using the natural-source magnetotelluric (MT) technique, as part of a variety of programs to study the craton and determine its regional-scale electrical structure. Two of the four types of surveys involved novel MT data acquisition; one through frozen lakes along ice roads during winter, and the second using ocean-bottom MT instrumentation deployed from float planes.

The primary initial objective of the MT surveys was to determine the geometry of the topography of the lithosphere–asthenosphere boundary (LAB) across the Slave craton. However, the MT responses revealed, completely serendipitously, a remarkable anomaly in electrical conductivity in the SCLM of the central Slave craton. This Central Slave Mantle Conductor (CSMC) anomaly is modelled as a localized region of low resistivity (10–15 Ω m) beginning at depths of ~ 80–120 km and striking NE–SW. Where precisely located, it is spatially coincident with the Eocene-aged kimberlite field in the central part of the craton (the so-called "Corridor of Hope"), and also with a geochemically defined ultra-depleted harzburgitic layer interpreted as oceanic or arc-related lithosphere emplaced during early tectonism. The CSMC lies wholly within the NE–SW striking central zone defined by Grütter et al. [Grütter, H.S., Apter, D.B., Kong, J., 1999. Crust–mantle coupling; evidence from mantle-derived xenocrystic garnets. Contributed paper at: The 7th International Kimberlite Conference Proceeding, J.B. Dawson Volume, 1, 307–313] on the basis of garnet geochemistry (G10 vs. G9) populations.

Deep-probing MT data from the lake bottom instruments infer that the conductor has a total depth-integrated conductivity (conductance) of the order of 2000 Siemens, which, given an internal resistivity of 10–15 Ω m, implies a thickness of 20–30 km. Below the CSMC the electrical resistivity of the lithosphere increases by a factor of 3–5 to values of around 50 Ω m. This change occurs at depths consistent with the graphite–diamond transition, which is taken as consistent with a carbon interpretation for the CSMC.

Preliminary three-dimensional MT modelling supports the NE–SW striking geometry for the conductor, and also suggests a NW dip. This geometry is taken as implying that the tectonic processes that emplaced this geophysical–geochemical body are likely related to the subduction of a craton of unknown provenance from the SE (present-day coordinates) during 2630–2620

* Corresponding author. Fax: +1-613-943-9285.
E-mail address: ajones@nrcan.gc.ca (A.G. Jones).
[1] Now at: Dublin Institute for Advanced Studies, 5 Merrion Square, Dublin 2, Ireland.

0024-4937/$ - see front matter
doi:10.1016/j.lithos.2003.08.001

Ma. It suggests that the lithospheric stacking model of Helmstaedt and Schulze [Helmstaedt, H.H., Schulze, D.J., 1989. Southern African kimberlites and their mantle sample: implications for Archean tectonics and lithosphere evolution. In Ross, J. (Ed.), Kimberlites and Related Rocks, Vol. 1: Their Composition, Occurrence, Origin, and Emplacement. Geological Society of Australia Special Publication, vol. 14, 358–368] is likely correct for the formation of the Slave's current SCLM.

Keywords: Slave craton; Magnetotelluric method; Archean tectonics; Canadian Shield; Electromagnetic survey; Geophysics

1. Introduction

The geological core of North America, the Canadian Shield, comprises an amalgam of Archean cratons and cratonic fragments welded together by Paleoproterozoic orogenies (Hoffman, 1988). A component of the Canadian Shield is the Slave craton (Fig. 1), in the northwestern part of the shield, that is approximately 600 km (N–S) × 400 km (E–W) in exposed areal extent and hosts the Acasta gneisses, currently the oldest dated rocks on Earth (4.027 Ga, Stern and Bleeker, 1998). In contrast to many other Archean cratons, excellent exposure has resulted in high quality geological bedrock maps being available. In addition, following Fipke's discovery of diamondiferous kimberlite pipes in the centre of the craton in 1991 (Fipke et al., 1995), the sub-continental lithospheric mantle (SCLM) structure of the craton has been, and is being, extensively studied both geochemically and geophysically.

In a Slave compilation published a decade ago, that predated the extraordinary diamond exploration activities of the 1990s, Padgham and Fyson (1992) contended that the Slave craton possesses several features that make it distinct compared to other Archean cratons, and particularly when compared to the Superior craton. These include high abundances of sedimentary rocks relative to volcanic rocks, high abundances of felsic to mafic rocks, high abundances of sialic basement, and high abundances of potassium-rich granite. Also strikingly is that a terrane classification, successfully applied to the Superior craton, cannot be as readily applied to the Slave craton. Kusky's (1989) attempt to do so has been demonstrated to be invalid through the mapping of a continguous single Mesoarchean (3.2–2.8 Ga) basement complex in the western half of the craton (the Central Slave Basement Complex) by Bleeker et al. (1999a,b).

Concomitant with detailed geological mapping of the surface of the Slave craton (Bleeker and Davis, 1999), which leads primarily to models for the formation of the Slave's crust, geochemical, geophysical and petrological studies have been undertaken over the last 5–10 years to image the Slave's SCLM with a view towards understanding its formation and evolution. The geophysical investigations included reflection profiling (Cook et al., 1999), a major refraction experiment (Viejo et al., 1999), teleseismic studies (Bostock, 1998; Bostock and Cassidy, 1997; Bank et al., 2000; Snyder et al., 2002), and a series of four magnetotelluric (MT) experiments. Geochemical studies of mantle samples have been undertaken by Kopylova et al. (1997), Cookenboo (1999), Griffin et al. (1999a,b), Grütter et al. (1999), MacKenzie and Canil (1999), Carbno and Canil (2002), and Heaman et al. (2002).

There are a number of competing models for the assembly of Archean lithosphere, with the proposed processes ranging from cycles of differentiation and collisional thickening (Jordan, 1988) to collision of island arcs comprising depleted material (Ashwal and Burke, 1989) to buoyant subduction and imbrication by lithospheric-scale stacks (Helmstaedt and Schulze, 1989; Kusky, 1989; Kusky and Polet, 1999) to basal accretion by cooling asthenospheric material (Thompson et al., 1996). Deep probing electromagnetic methods are particularly well suited for constraining lithospheric structure (Jones, 1999) as electrical conductivity is influenced by both thermal state and compositional variations. In particular, high precision MT data can resolve the depth to the lithosphere–asthenosphere boundary (LAB) to better than 10% (see, e.g., Jones, 1999), as electrical conductivity rises by two or more orders of magnitude at the initiation of even very low orders of partial melt (0.1%) due to the efficient interconnectivity of the melt (Nakano and Fujii, 1989; Minarik

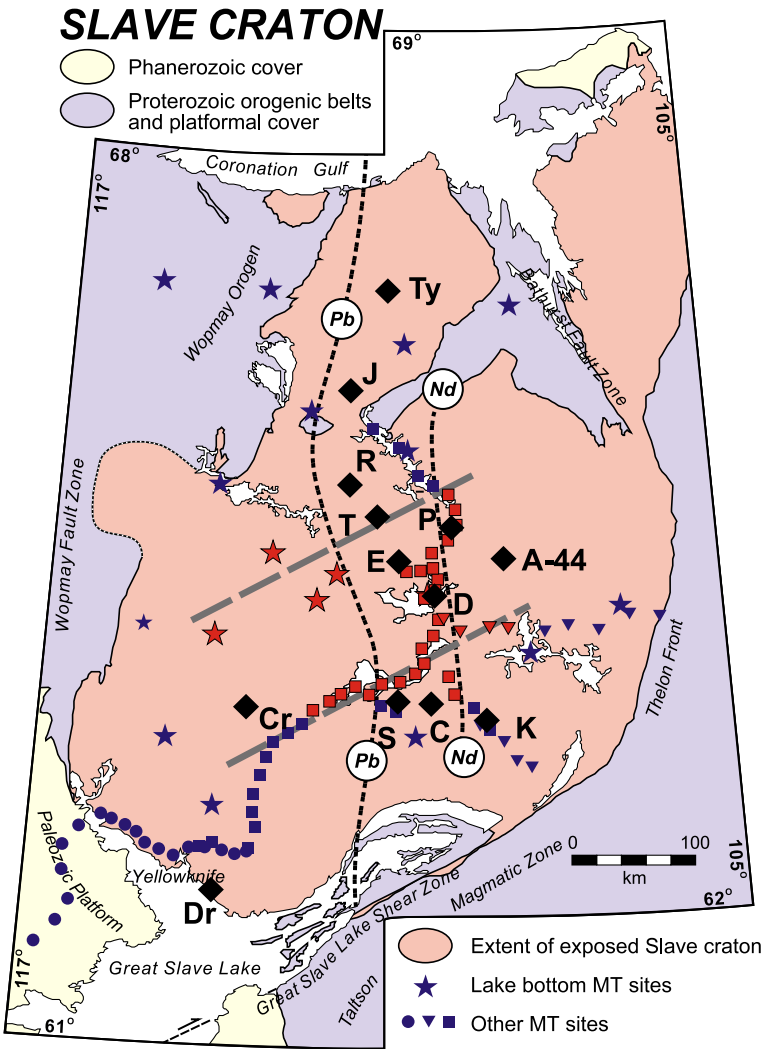

Fig. 1. The Slave craton together with the locations of the MT sites. Dots: 1996 all-weather road sites. Squares: 1998, 1999 and 2000 winter road sites. Stars: 1998–1999 and 1999–2000 lake bottom sites. Significant kimberlite pipes (diamonds): Dr: Drybones; Cr: Cross Lake; S: Snap; C: Camsell; K: Kennady; D: Diavik pipes; E: Ekati mine; P: Point Lake; A-44; A-44 pipe; T: Torrie; R: Ranch; J: Jericho; Ty; Tenacity. Also shown are the north–south Pb and Nd isotope boundaries and the geochemical boundaries of Grütter (two grey dashed lines projecting NE–SW). MT sites in red are those lying above the Central Slave Mantle Conductor.

and Watson, 1995; Drury and Fitz Gerald, 1996; Schilling et al., 1997).

In this paper we discuss electrical resistivity models obtained from deep-probing electromagnetic surveys of the Slave craton using the natural-source magnetotelluric (MT) technique. In total, MT measurements have been made at 138 locations across the craton, predominantly in the southern half. Three previous publications discuss the interpretation of subsets of these data. Jones and Ferguson (2001) concentrate on the data from west of Yellowknife, and show that the seismically defined base of the crust correlates with a step-like change in electrical resistivity. Jones et al. (2001a) discuss the first results of the craton response from the Slave, focussing on the discovery of a conductive anomaly in the upper mantle beneath the central part of the craton, named the Central Slave Mantle Conductor (CSMC). Finally,

Wu et al. (2002) discuss the MT data crossing the Great Slave Lake shear zone (Fig. 1), which forms the southern boundary of the Slave craton. Herein we present one-dimensional (1-D), two-dimensional (2-D) and three-dimensional (3-D) resistivity models from the craton. The CSMC is shown in 3-D to have a NE–SW strike, and a NW dip, and lie at a depth of ~ 80–100 km. As shown previously, it correlates spatially with the Eocene kimberlite magmatism, and with a geochemical zonation of the Slave based on garnet geochemistry (G10 vs. G9) populations.

We interpret the CSMC as due to carbon, either as graphite or as carbon on grain boundary films, as a relic of Neoarchean (2.8–2.5 Ga) tectonism during which an exotic terrane underplated the craton from the SE (in present-day coordinates). Craven and Jones (2001) discussed the redox conditions that likely resulted in the precipitation of carbon in the upper mantle, and Davis et al. (2003) explore tectonic implications further by compiling information from a variety of sources that all infer a three-part zonation of the Slave's sub-continental lithospheric mantle (SCLM).

2. Magnetotelluric method and experiments

2.1. Magnetotelluric method

The magnetotelluric (MT) method is based on measurement of the electromagnetic (EM) effects of electric currents induced in Earth by natural external sources, such as world-wide lightning activity and the interaction of solar plasma, from solar flares, with the Earth's magnetosphere (Vozoff, 1991). At the frequencies used (typically 20 kHz to 0.0001 Hz, or periods of 0.0005 to 10,000 s), EM propagation is mathematically described by a diffusion equation rather than a wave equation. However, although at these low frequencies the EM fields propagate diffusively, there are significant differences in the technique compared to diffusion by thermal, gravity or static magnetic fields. In particular, there are formal uniqueness solutions to the MT equations for one-dimensional (1-D) (Bailey, 1970) and two-dimensional (2-D) (Weidelt, 2000, pers. comm.) Earths. Unlike potential field methods, the MT method is not inherently non-unique. In particular, as a consequence of frequency dependence (the *skin depth* effect), MT data have the ability to resolve depth information.

In the MT method, time-varying components of the EM field are measured at the Earth's surface; all three components of the magnetic field (*Hx*, *Hy* and *Hz*) and the two horizontal components of the electric field (*Ex* and *Ey*), where *x* and *y* usually denote north and east, respectively. These components are related to each other through frequency-dependent, complex *transfer functions*. The relationship between the horizontal electric and magnetic field components are described by the 2×2 MT *impedance tensor*, $\boldsymbol{Z}(\omega)$, and between the vertical magnetic field component and the horizontal magnetic field components by the *geomagnetic transfer function*, $\boldsymbol{T}(\omega)$.

The elements of the MT impedance tensor are transformed so that their scaled magnitudes give the correct resistivity for a uniform half space. The real and imaginary parts of the elements of $\boldsymbol{T}(\omega)$ are plotted as induction arrows, where by convention the real arrows are usually reversed to point towards regions of current concentration (Parkinson, 1962; Jones, 1986). Further description of the MT method can be found in Vozoff (1986, 1991) and Jones (1992, 1993, 1998, 1999).

2.2. Magnetotelluric experiments

Three types of MT experiments have been conducted on the Slave craton since 1996. The types of instruments used, and their observational range, are listed in Table 1, the surveys, with dates and numbers of sites, are listed in Table 2 and the sites are plotted in Fig. 1. In total, MT measurements have been made at 138 locations across the craton, with the majority being in the southern third of the craton.

The land-based surveys involved deployments of conventional MT acquisition. The initial MT survey, in Autumn 1996, comprised broadband acquisition using both V5 and LiMS instruments every 10 km along the only all-weather road on the craton (filled dots in Figs. 1 and 6). This profile is located in the SW corner of the Slave running E–W approximately 100 km either side of the city of Yellowknife (Fig. 1). The 2000 Targeted Geoscience Initiative (TGI) survey consisted of long period systems at 15 locations installed by helicopter and float plane (inverted triangles in Figs. 1 and 6).

Table 1
Details of the MT instrumentation used

Name	Manufacturer	Frequency range (period range)	Deployment time
V5	Phoenix Geophysics	10,000–0.00055 Hz (0.0001–1820 s)	3 nights
V5-2000	Phoenix Geophysics	384–0.00055 Hz (0.0026–1820 s)	2 nights
GMS-06	Metronix	AMT range: 10,000–10 Hz, MT range: 200–0.0005 Hz (0.005–1860 s)	3 nights
LiMS (Long Period MT System)	Geological Survey of Canada	0.05–0.0001 Hz (20–10,000 s)	4 weeks
OBMT (Ocean Bottom MT)	Woods Hole Oceanographic Institution	0.012–0.00004 Hz (85–26,000 s)	1 year

The winter road surveys (squares in Fig. 1) comprised unconventional MT acquisition during wintertime along the ice roads of the Slave craton that are used to supply various exploration and mining camps. The procedure involved separate acquisition of the electric and magnetic fields, with the five electric field sensors (electrodes) being lowered to the bottoms of lakes through holes cut through the ice. Magnetic acquisition directly on the ice of the lakes was severely contaminated by ice movement at 10–100 s periods (McNeice and Jones, 1998), so the magnetometer sensors were installed on the nearest shoreline. Fortuitously, the first winter road survey, in 1998, coincided with the completion of development of a new generation 24-bit MT acquisition system with separate electric and magnetic field recorders, and this survey was the first conducted using these systems by Phoenix Geophysics.

The two lake bottom surveys employed low-power instruments designed for deployment on the continental shelf (Petitt et al., 1994) that were installed and recovered by Twin Otter float planes (stars in Figs. 1 and 6). The electrode chemistry was modified to suit fresh water installation, but no other instrument changes were required for this application. The instruments were deployed in August of each year when the lakes were not ice covered, then retrieved the following July. The digitising rate was set at 2.8 s for the first month, then automatically changed to 28 s for the remaining 10 months. Ten instruments were deployed twice at the 19 locations in Fig. 1, with a year's recording at each location. Some data losses occurred for the electric field systems, but in all cases the magnetic fields were recorded. The orientation on the lake bottom was determined through weekly measurements of a recording compass.

2.3. Data processing

Data processing involved rotating the measured time series into geographic coordinates and estimating the MT response functions relating the horizontal electric field components to the horizontal magnetic field components and the vertical field transfer functions (TF) relating the vertical magnetic field component to the horizontal magnetic field components. The codes used were robust, multi-remote reference codes of Jones (Jones and Jödicke, 1984; method 6 in Jones

Table 2
MT surveys

Date	Style	Major funding agencies	Instrumentation	Number of sites
1996 July–September	Land	LITHOPROBE	V5	60 (13 on craton)
		GSC	LiMS	56 (12 on craton)
1998 March–April	Winter road	LITHOPROBE	V5-2000	12
		GSC	LiMS	11
1999 March–April	Winter road	LITHOPROBE	V5-2000	19
		GSC	LiMS	18
2000 March–April	Winter road	LITHOPROBE	GMS-06 – MT	12
		GSC	LiMS	12
2000 April	Winter road	GSC (EXTECH-III)	GMS-06 AMT + MT	8
2000 July–August	Land (helicopter)	GSC (TGI)	LiMS	15
1998–1999 August–July	Lake bottom	NSF, LITHOPROBE	OBMT	9
1999–2000 August–July	Lake bottom	NSF, LITHOPROBE	OBMT	9

et al., 1989) and Chave and Thomson (2003). Additionally, data segments were selected with low vertical field variations in order to avoid source field effects on the data (Garcia et al., 1997; Jones and Spratt, 2002).

3. Average 1-D craton electrical structure

An estimate of the average 1-D electrical structure of the craton can be obtained by averaging the MT responses, in both azimuthal directions, from all sites on the craton. At each site and frequency, the azimuthal average is obtained from the arithmetic average of the response in the two orthogonal directions, the so-called Berdichevsky, or arithmetic, average (Berdichevsky and Dmitriev, 1976). This estimate is rotationally invariant so is not biased by the orientation of the deployment. Given that the different MT systems resulted in MT impedance tensor estimates with different period sets, the data from the 138 sites were averaged into period bins that were 1/6 of a decade wide. For both the log(apparent resistivity) and phase data, the averages were obtained robustly by determining the median values within each bin. (A lognormal distribution for apparent resistivities was shown by Bentley, 1973.) Conservative estimates of variance were obtained using jackknife methods (Chave and Thomson, 2003), and the 95% confidence intervals were calculated assuming a Student-*t* distribution for the variances (e.g., Bendat and Piersol, 1971, p. 112).

The resulting craton-average MT responses are shown in Fig. 2 (solid circles). There is a visible "tear" in the apparent resistivity curve at periods above and below 0.0025 s (400 Hz). This is because

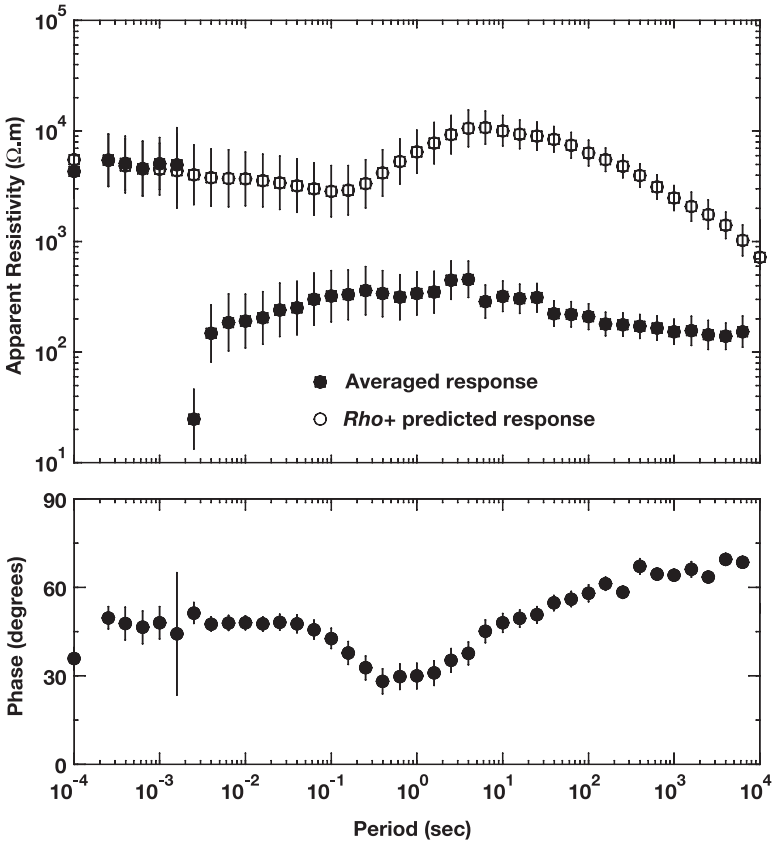

Fig. 2. Averaged Slave MT response (solid circles), with predicted apparent resistivity curve (open circles) using Parker and Booker's (1996) *Rho*+ algorithm.

the only high frequency responses come from the land-based sites close to Yellowknife on the Anton complex of the Central Slave Basement Complex, a region with little conducting material in the crust (Jones and Ferguson, 2001). The majority of the Slave stations were located either in lakes (OBMT) or with the electrodes on the lake bottoms (winter road surveys). The accumulation of till on the lake bottoms causes a downward shift of the apparent resistivity curves. This is called the *static shift* effect (Jones, 1988; Sternberg et al., 1988), and is caused by the electrical charges on the boundaries of the till reducing the amount of electric field. In contrast, the phases do not suffer from distortions due to these charges, and accordingly the lateral phase variations are reasonably smooth.

This problem with static shifts associated with three-dimensional geometries means that not only is the actual level in question, but that the *shape* of the apparent resistivity curve could be distorted. This can be tested by predicting the apparent resistivity curve from the phase data, using the *Rho*+ algorithm of Parker and Booker (1996). Assuming that the highest frequency apparent resistivity values are at the correct level, then the predicted apparent resistivity data are those shown by the open circles in Fig. 2. The error estimates are 95% confidence intervals derived from the *Rho*+ prediction. Using Parker's *D*+ analysis, which yields the best possible fitting layered (1-D) model (Parker, 1980; Parker and Whaler, 1981), demonstrates that a normalized RMS (root mean square) misfit of 0.58 is the lowest possible for the open circle data in Fig. 2 (statistically, a value of unity is desired). However, the largest misfit is on the longest period value (10,000 s); deleting these apparent resistivity and phase data results in a minimum possible normalized RMS misfit of 0.34. This suggests that the conservative error estimates for the averaged means of apparent resistivity are, on average, a factor of three too large.

The measured phase data together with the measured high frequency apparent resistivities and the low frequency predicted apparent resistivities can be inverted to estimate the average 1-D structure of the craton. The 1-D layered-Earth algorithm of Fischer et al. (1981) yields a five-layer model with a moderately resistive upper crust, a resistive lower crust and upper mantle to $\sim$90 km, then a moderately resistive mantle underlain by more conducting mantle layers at some hundreds of kilometres. The best-fitting five-layer model, derived using the minimization scheme of Fischer and Le Quang (1981), has a reduced RMS misfit of 0.32. The best-fitting four-layer model has a reduced RMS misfit that is a factor of five larger, and the best-fitting six-layer model has a reduced RMS misfit that is 5% larger. Thus, a five-layer model represents the minimum number of homogeneous layers that can fit the data.

Still in doubt however is the correct level of the apparent resistivity curve that in Fig. 2 was defined by the highest frequency response from the sites on the resistive Anton complex. This level affects both the resistivities and the layer depths of the 1-D model. Given the suggestion of a step change in resistivity at the base of the crust by Jones and Ferguson (2001), the apparent resistivity data can be scaled to result in the interface at 88 km rising to the average Moho depth for the craton. From the teleseismic work of Bank et al. (2000), and the more recent studies by Snyder et al. (2002), the Moho thickness varies across the craton from a maximum of 46 km at the southeast, to a minimum of 37 km in the northwest (see Davis et al., 2003), with an average depth of around 40 km. Scaling the apparent resistivity curve to result in an interface at 40 km requires that the data be shifted by a factor of $(40/90)^2$, or $\sim$0.2 (Jones, 1988).

The shifted curve is shown in Fig. 3, together with the 1-D model that fits this curve. The parameters of the model are listed in Table 3. Sensitivity analysis, using singular value decomposition (Edwards et al., 1981; Jones, 1982), shows that the eight model parameters (five layer resistivities, ρ, and three depths, d, with one depth (d_2 = Moho) held constant) are all resolved, in the order ρ_1, d_3, ρ_3, d_1/ρ_5, h_1, h_4, ρ_2 with ρ_4 being least well resolved. The standard deviation ranges of the model parameters are also listed in Table 3. The smoothest model that fits the data, to within 10% of the minimum possible misfit (i.e., 0.37), is also shown in Fig. 3. This smooth model trades off finding the best-fitting model with minimizing the vertical gradient in resistivity (Constable et al., 1987). Converting the responses from apparent resistivities to Schmucker's *C* response (Schmucker, 1970) shows that the maximum depth of penetration, given by the maximum eddy current flow (Weidelt, 1972), is ap-

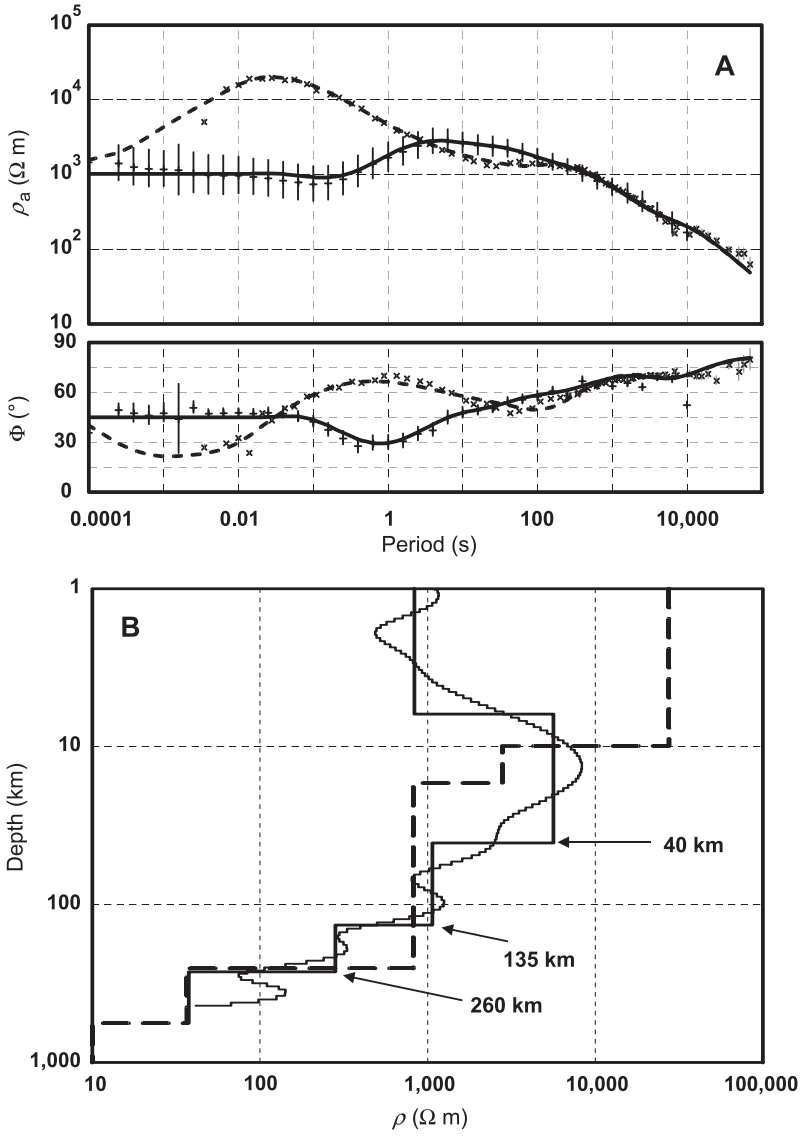

Fig. 3. Modified averaged Slave MT responses with 95% error bounds together with the layered-Earth (solid line) and smooth (light solid line) models that best fit the responses (pluses). Also shown are the MT responses from the central part of the Superior craton (crosses) obtained by Schultz et al. (1993), and their best-fitting layered-Earth model (dashed line).

proximately 300 km. Thus, the data should, on average, penetrate through the sub-continental lithospheric mantle in its entirety.

The inference from the average MT response is that the lithosphere across the Slave is, on average, some 260 km thick. This is consistent with the petrologically defined lithospheric thickness, from analyses of mantle xenoliths, of 260 km for the southern part of the craton (Kopylova, 2002), but is thicker than the petrologically defined lithospheric thicknesses of 190–200 km for the northern Slave (Jericho, Kopylova et al., 1997) and central Slave (Lac de Gras pipes, Pearson et al., 1999). The majority of the MT sites on the Slave used for this average are located on the southern part of the craton, so there is an inherent bias towards deeper thicknesses for the lithosphere.

Table 3
Parameters of scaled 1-D Slave craton model

Layer	Resistivity (Ω m)	Depth to base (km)
Layer 1: Upper crust	850 (750–950)	6 (4.2–8.6)
Layer 2: Lower crust	5300 (3400–8200)	40 (fixed)
Layer 3: Upper SCLM	1100 (870–1400)	130 (95–185)
Layer 4: Lower SCLM	300 (150–600)	260 (225–310)
Layer 5: Asthenosphere	75 (55–95)	

3.1. Lac de Gras response

Below we discuss the conductivity anomaly discovered in the central part of the Slave craton, which we name the Central Slave Mantle Conductor (CSMC). Due to the presence of this conductor, the incident fields at the longest periods of the winter road data in the middle of the craton do not penetrate through the CSMC with sufficient energy to determine the structure of the mantle below. However, the responses derived from the 1 year of data from the Lac de Gras (Fig. 1) lake bottom site are of high quality to ~ 8000 s, and have a penetration depth of ~ 250–300 km, based on Weidelt's (1972) depth of maximum eddy current flow, and 257 km from Parker's *D*+ model (Parker, 1980; Parker and Whaler, 1981). Fig. 4 shows the averaged apparent resistivity and phase MT curves from the Lac de Gras lake bottom site. Note that the phases are plotted on an expanded scale of 60–90° compared to Figs. 2 and 3. The phase curve displays a subtle minimum at periods of 500–3000 s, which are the periods sensitive to resistivity at depths of the order of 120–200 km. Also shown in Fig. 4 are two smooth models that fit the response to an RMS of 0.90; one model is a continuously smooth model, whereas the other allows a step-change in resistivity at the petrologically defined base of the lithosphere at ~ 200 km (Pearson et al., 1999). Both models show a resistivity minimum within the SCLM of 13 Ω m at a depth of 123 km, consistent with the CSMC. The *D*+ analysis suggests that the data are best fit with a conducting zone centered on 128 km with a depth-integrated conductivity (conductivity–thickness product) of ~ 2000 Siemens. For an internal resistivity of 13 Ω m, the conducting anomaly is 26 km thick, ranging over 115–141 km in extent.

At greater depths resistivity increases to a value of ~ 50 Ω m, then decreases sharply to a poorly defined value but < 5 Ω m. Sensitivity analysis of a layered Earth model that fits the data, with interfaces at 40 km (base of crust), 115 km (top of conducting layer), 141 km (base of CSMC), and 200 km (base of lithosphere), shows that the internal resistivity of the CSMC is in the range 10–15 Ω m, and the underlying deep lithosphere resistivity in the range 17–141 Ω m. We take this fourfold increase in resistivity as the transition out of the CSMC conducting anomaly with depth, and interpret it as evidence for a change in electrical properties of carbon when crossing the graphite–diamond stability field.

The base of the lithosphere is suggested by Parker's *D*+ model to be 210 km where a conductance of 13,000 Siemens is seen. This is consistent with the 200 km value for lithospheric thickness reported by Pearson et al. (1999).

3.2. Comparison with the Superior craton

Fig. 3 shows the average response for the Slave craton, after scaling the MT apparent resistivity curve to give an interface at 40 km (see above), with that for the central part of the Superior craton obtained by Schultz et al. (1993). The MT responses obtained by Schultz et al. (1993) are the most precise for any craton, and indeed for mantle-probing depths anywhere in the world, and are the result of 2 years of acquisition using a large electrode array (1 km long lines) in a lake (Carty Lake) in the Kapuskasing region of northern Ontario, Canada. The crust of the Kapuskasing region is geologically highly complex, but very simple in its electrical response (Kurtz et al., 1993), thus providing an excellent window on the mantle below. Due to the high precision of the Carty Lake MT response estimates, the models obtained from them have high resolving power.

Astoundingly, the Slave and Superior phase responses coalesce at periods of 30 s, and the apparent resistivity responses coalesce at a period of 300 s. This suggests that whereas the crustal and upper SCLM electrical structures are clearly different between the two cratons, on average the deeper mantle of the two is the same electrically. The two apparent resistivity curves were scaled in very different ways: the Slave apparent resistivity curve is scaled to result in an interface at the crust–mantle interface, whereas the Superior apparent resistivity curve was scaled to be consistent with observations from nearby geomagnetic

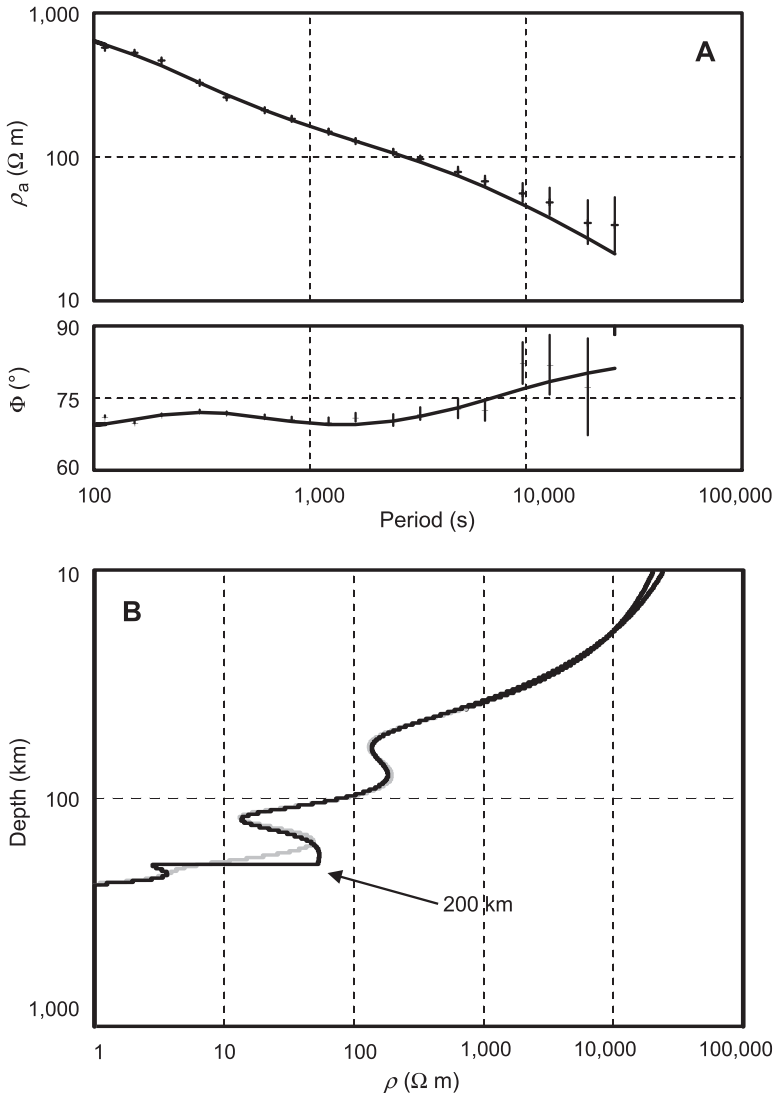

Fig. 4. MT responses from the lake bottom instrument installed in Lac de Gras together with the smooth models that best-fit the responses. One model has no interfaces, whereas the other permits a step-change in resistivity at 200 km depth (base of the lithosphere).

observatories. That these two scalings result in the same apparent resistivity at long periods suggests that the approach used on the Slave data is valid.

The layered-Earth model, with the minimum acceptable number of homogeneous layers, that fits the Superior response is also shown in Fig. 3, and can be compared with the Slave model. Both show a step-change in resistivity at 250–260 km. Given the high precision of the responses from the Superior craton, the thickness of the lithosphere can be far more precisely determined than for the Slave, and linear sensitivity SVD analysis suggests that it is 253 ± 6 km, with asthenospheric resistivity of 37 ± 7 Ω m. The statistical uncertainty in the base of the lithosphere of ± 6 km is correct under the assumption of a layered 1-D Earth with discrete resistivity changes. If the lithosphere–asthenosphere boundary zone is transitional electrically, then it can occur over more like 50 km (see, e.g., Cavaliere and Jones, 1984). However, laboratory studies suggest that a decrease of >1.5

orders of magnitude in resistivity occurs for a 50 °C change in temperature at the onset of partial melting (Partzsch et al., 2000), and, for a typical continental cratonic geotherm valid for the Slave craton (e.g., Kopylova et al., 1997), a 50 °C change will occur over <20 km.

The resistivity in the deep lithosphere is consistent with a reduced water content compared to tectonically activated or oceanic lithosphere, which may play a role in stabilizing Archean lithosphere against convective erosion (Hirth et al., 2000).

4. Phase maps

MT phase maps are an excellent qualitative indicator of structure, as MT phase is unaffected by electric galvanic distortion that can plague apparent resistivity estimates. Fig. 5 shows phase maps for six periods over the 30 to 10,000 s band, which represent increasing depth penetration within the lithospheric mantle. The phase contoured is the arithmetic (Berdichevsky) average of the two orthogonal phases, and is a rotationally invariant phase. Also shown on the maps are the locations of the geochemically defined mantle domain boundaries of Grütter et al. (1999), and the Pb and Nd isotope boundaries of Thorpe et al. (1992), Davis and Hegner (1992) and Davis et al. (1996).

A coarse guide to the approximate penetration depths of these MT phase maps can be derived from the averaged craton response discussed above. Weidelt's depth of maximum eddy current flow are: 30 s ≈ 65 km; 100 s ≈ 110 km; 300 s ≈ 165 km; 1000 s ≈ 240 km; 3000 s ≈ 310 km; and 10,000 s ≈ 335 km. However, such conversion must be treated with caution, as the highly non-linear mapping from period to depth is a function of the subsurface resistivity and can vary wildly across the map area given the vast range of electrical resistivity. This is particularly true for data from sites located on top of the CSMC; the conductor absorbs and attenuates the EM fields restricting penetration strongly.

The averaged phase data have been smoothed using the nearest neighbour algorithm implemented in the Generic Mapping Tools (GMT) package (Wessel and Smith, 1991). The 30 and 100 s maps have a different colour range than the other maps, from 45° to 75° rather than from 55° to 85°. There are no 30 s data from the lake bottom sites, and, conversely, the 10,000 s map is almost entirely dictated by the lake bottom responses.

There is a marked increase in phase between the 30 s map and the 100 s map for sites in the centre of the craton lying predominantly within the mantle zone boundaries defined by Grütter et al. (1999). This is caused by the presence of the Central Slave Mantle Conductor (CSMC). High phases are also observed at the eastern boundary of the Slave; these are due to the conducting material within the Thelon orogen (Jones et al., 2001b). Comparing the maps for 300 and 1000 s, a clear NW shift in phases is apparent. This we interpret as evidence for a NW-dip to the CSMC. Note that at these mantle-probing periods, the data do not respect the Pb and Nd isotope boundaries, suggestive of a mantle geometry that is at a high angle to the dominant crustal tectonic boundaries. This dichotomy between the crustally defined structures and those defined for the Slave's sub-continental lithospheric mantle on the basis of petrological, geochemistry and geophysical data is discussed further in Davis et al. (2003).

At the longest periods of 3000 and 10,000 s, there is no clear pattern to the phases, save the suggestion of an east–west difference. At this stage we do not ascribe any significance to this apparent correlation, as it requires further verification from more detailed analyses of the longest period data. In particular, the 10,000 s map may be affected by source field effects (Garcia et al., 1997; Jones and Spratt, 2002).

5. Two-dimensional models

Two-dimensional (2-D) models have been derived for four profiles crossing the Slave province. The locations of the profiles are shown in Fig. 6, together with the locations of the mantle domain boundaries defined by Grütter et al. (1999) and the Pb and Nd isotope boundaries of Thorpe et al. (1992), Davis and Hegner (1992) and Davis et al. (1996). These models were derived independently of each other; further work will occur to ensure the same resistivity structures at intersection points. For all models, strike direction was taken to be perpendicular to the profile direction. This assumption may lead to less resolution

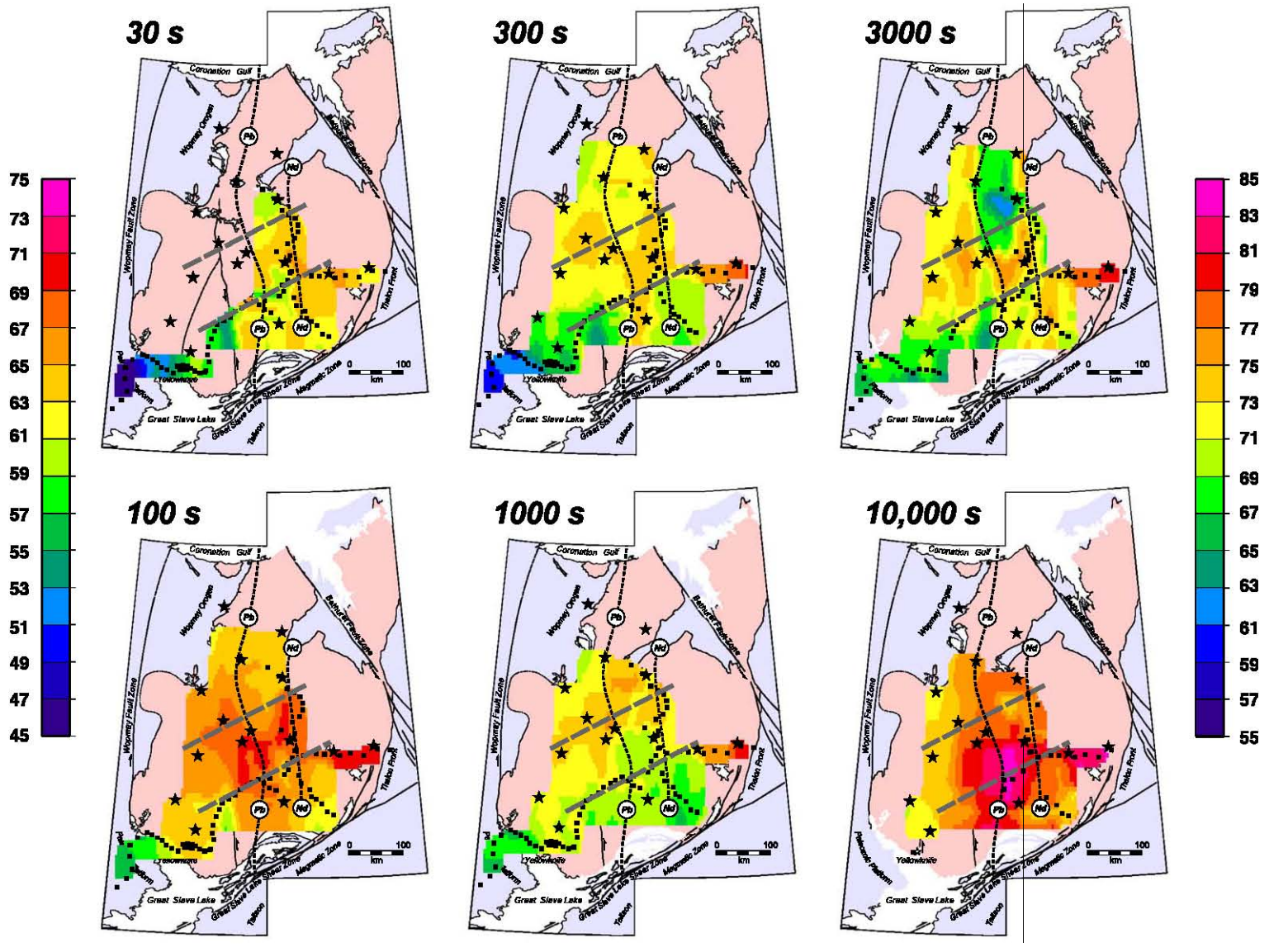

Fig. 5. Contoured averaged phase maps for periods from 30 to 10,000 s. The phases in the shortest frequency maps (30 and 100 s) range from 45° to 75°, whereas the phases in the other four maps range from 55° to 85°.

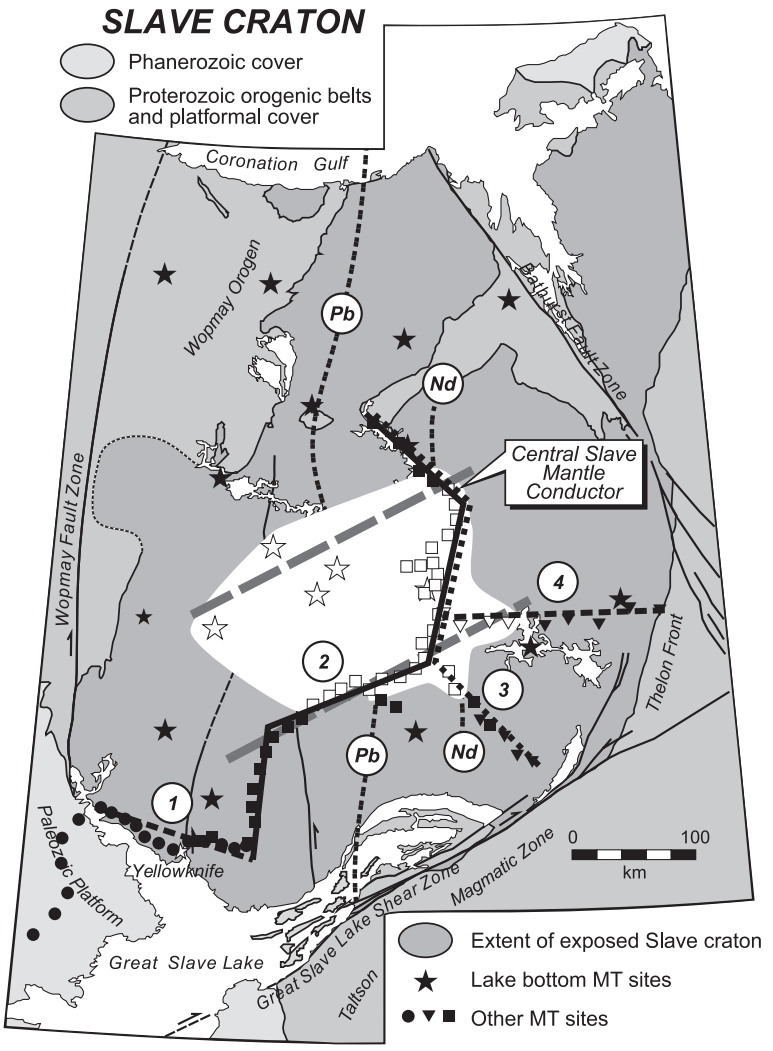

Fig. 6. The Slave craton together with the locations of the MT sites and the four model profiles. Dots: 1996 all-weather road sites. Squares: 1998 and 1999 winter road sites. Named stars: 1998–1999 and 1999–2000 lake bottom sites. Inverted triangles: 2000 TGI sites. The open MT symbols (squares, inverted triangles and stars) designate sites on top of the CSMC. Also shown are the north–south Pb and Nd isotope boundaries and the geochemical boundaries of Grütter et al. (1999).

than possible in the models, but should not cause erroneous structure as the mantle resistivity structure in the SCLM is slowly varying laterally. Virtually the same results could have been obtained from stitching together 1-D models from all the sites.

Profile 1 is an ~150-km-long E–W profile along the all-weather road in the SW part of the craton from Rae in the west to Tibbit Lake at the eastern end of the Ingraham Trail, with the city of Yellowknife at the centre. Profile 2 follows the winter road from Tibbit Lake at its southern end to the Lupin Mine on the NW end of Contwoyto Lake. It runs north from the eastern end of Profile 1 to the north end of Gordon Lake, where it kinks to the NW along MacKay Lake, then north through the Lac de Gras region to the southern end of Contwoyto Lake, then NW along Contwoyto Lake. Profile 3 starts in the SE part of the Slave at the Kennady exploration property of De Beers and Mountain Province ("K" in Fig. 1), and goes NW until it joins up with Profile 2 at MacKay Lake. Profile 4 runs

directly east from the winter road across the northern arm of Aylmer Lake to the eastern boundary of the Slave craton, which is the Thelon orogen.

The models for all four profiles are shown in Fig. 7. The hotter colours represent regions where there are interconnected conducting phases, whereas the colder

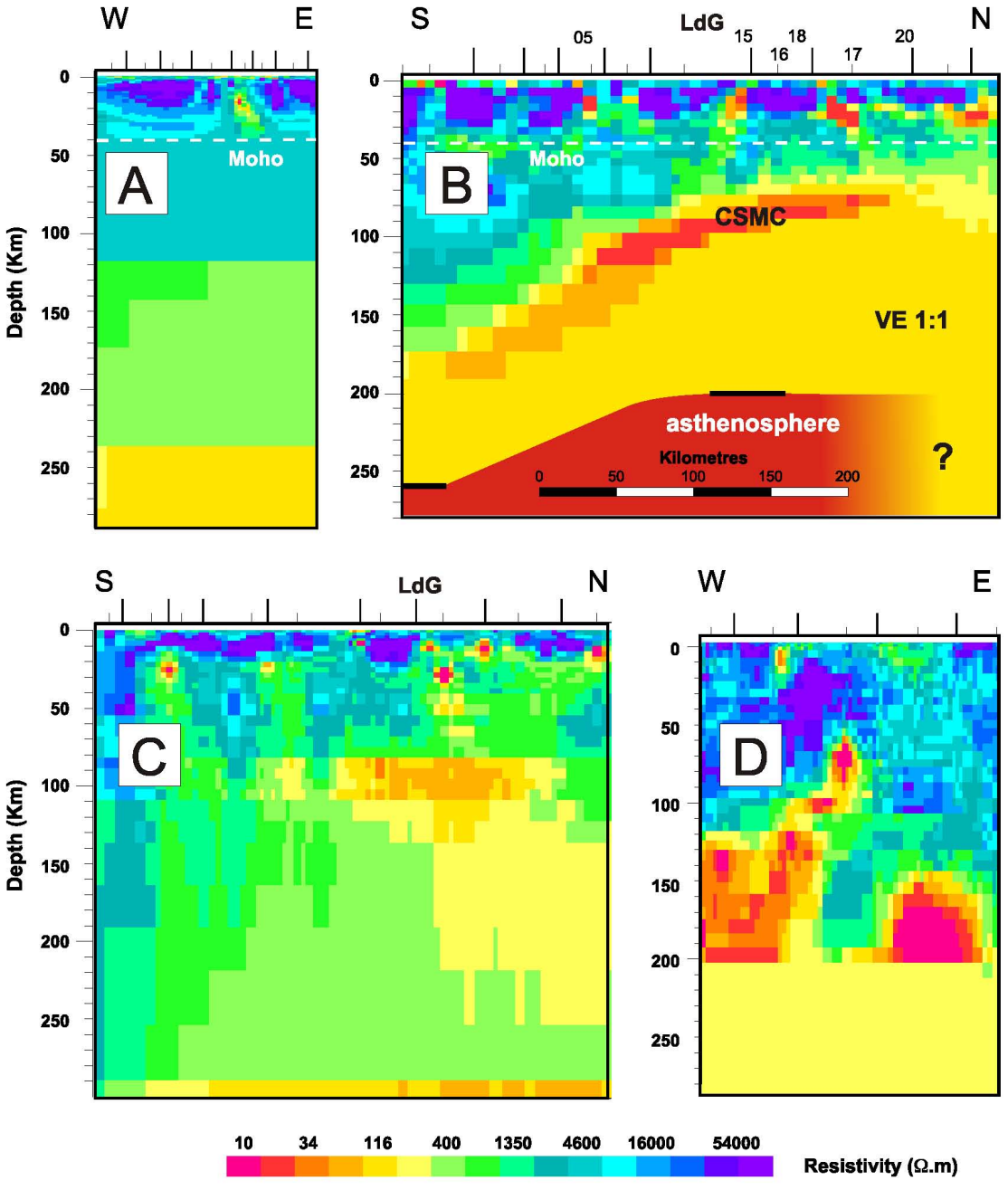

Fig. 7. Two-dimensional models along the four profiles shown in Fig. 6. A = Profile 1; B = Profile 2; C = Profile 3; D = Profile 4. All models plotted with a VE of 1:1 and with the same colour scale.

colours represent regions where conducting material is absent. The models were all obtained using Mackie's RLM2DI code (Rodi and Mackie, 2001), as implemented within the Geotools package, fitting both the strike-parallel (TE-mode) and strike-perpendicular (TM-mode) MT responses simultaneously. The inversion approach is to overparameterize the model, then search for the smoothest model that fits the observations, as pioneered in MT initially in 1-D by Constable et al. (1987), trading off misfit with smoothness using Tikhonov regularization (Tikhonov and Glasko, 1975). The start models for the inversions were either uniform half-spaces, or a layered Earth model based on the 1-D model presented in Fig. 3. The models were all fit to an average misfit of $\sim 5^\circ$ in phase, with a higher misfit on apparent resistivity permitted (25%) to account for static shifts.

Focussing on the SCLM structure, there is a consistent image from profile-to-profile. In the south, there are no significant conducting anomalies in the SCLM, The only crustal anomaly is a region of reduced resistivity to the east of Yellowknife on Profile 1 (Fig. 7A), which may be associated with the mineralisation observed along the Yellowknife fault (Garcia and Jones, 2000). Apart from that anomaly, the crust and SCLM are resistive, and there appears to be a discontinuity at the base of the crust (Jones and Ferguson, 2001). In agreement with the 1-D models, the depth of the base of the lithosphere is of the order of 250 km.

The 2-D model obtained for the data along Profile 2 (Fig. 7b) has been presented and discussed by Jones et al. (2001a), and is included here for completeness. The addition made here is that the area previously described as "region of no penetration" in Fig. 3 of Jones et al. (2001a) has now been sampled by the long period lake bottom data (Fig. 4), and shown to be of higher resistivity than the conductor. Also, the LAB is suggested to be at ~ 200 km. To the north, commencing beneath station 05, there is an upper mantle conducting region that exists to the southern end of Contwoyto Lake (between stations 17 and 20). This Central Slave Mantle Conductor (CSMC) begins at a depth of around 80–100 km, and has an internal resistivity of 30 Ω m or less, with a value of 13 Ω m suggested by the 1-D smooth modelling (Fig. 3).

The model for Profile 3 (Fig. 7C) shows a localized conducting anomaly within the SCLM at a depth of ~ 85 km. It begins to the south at the intersection of the Kennady Lake road and the main winter road, and continues to the southern end of Contwoyto Lake, consistent with the model for Profile 2.

The Profile 4 model (Fig. 7D) also exhibits evidence for the mantle conductor existing as far to the east as the northern arm of Aylmer Lake. There is an apparent conductor deep in the mantle at the eastern end of the line, but this is an artefact caused by the presence of conducting material within the crust of the Thelon orogen to the east, as clearly indicated by the induction arrows (Jones et al., 2001b).

6. Three-dimensional model

A 3-D resistivity model is being developed to explain the MT and TF observations. Herein we present the current version that describes qualitatively the major features predominantly in the TF data. Further work will be undertaken, including 3-D inversion, to fit all available MT and TF data, but we do not anticipate significant changes in the major features and geometries of the final model from the one we present here. The model was constructed by trial-and-error attempting to fit qualitatively the magnetic transfer functions, and some aspects of the MT responses, from the bottom lake sites and some selected winter road sites. Taken into account also were the general background resistivities observed in the 2-D models discussed above. The a priori information regarding the conductive 3-D features has been obtained from the results of a tensor dimensionality analysis scheme, developed by Lezaeta and Haak (2003), which indicates that the long period MT data suggest the existence of an anomalous SW–NE striking 3-D conductor at depth. Sites close to the Thelon Front (site HEA in Fig. 6) are affected by 3-D induction and also by strong current channelling. Both 3-D induction and current channelling effects can be explained with a model of dyke-like conductors of limited lateral extent or anisotropic conductive structures embedded in a more resistive crust (Lezaeta and Haak, 2003).

The model was built using the Geotools model builder, and its forward response was calculated using the code of Mackie and Madden (1993) and Mackie et al. (1993, 1994), with the recent modifi-

cations (bi-conjugate gradient stabilized method using an incomplete cholesky decomposition with a new scheme for updating the divergence of the H fields resulting in extremely fast convergence of the solution.) by R.L. Mackie and J.R. Booker (2001, pers. comm.). The model consists of 65 cells in the north direction, 62 cells in the east–west direction, and 24 cells vertically.

A horizontal slice at a depth of 140 km through the 3-D model is shown in Fig. 8, using approximately the same colour scheme as the 2-D models in Fig. 7. Also shown on the figure are the observed (solid arrows) and calculated (open arrows) real induction vectors at a period of 620 s for the lake bottom sites and some selected land and winter road sites. (This period is longer than that for the MT responses as the TF data

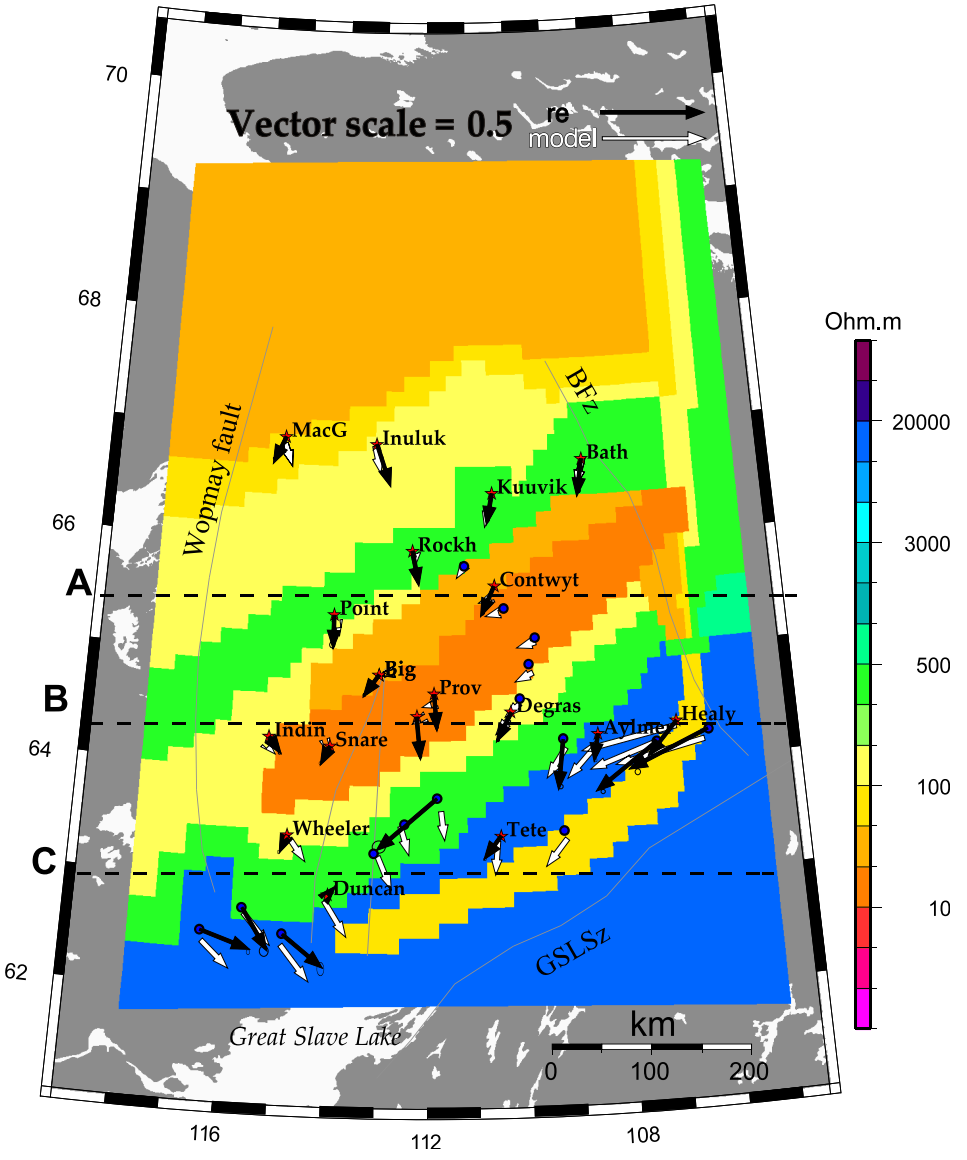

Fig. 8. Horizontal slice of the 3-D resistivity model at 140 km depth. The vectors are the unreversed induction arrows of the measured data (solid arrows) and the calculated data (open arrows).

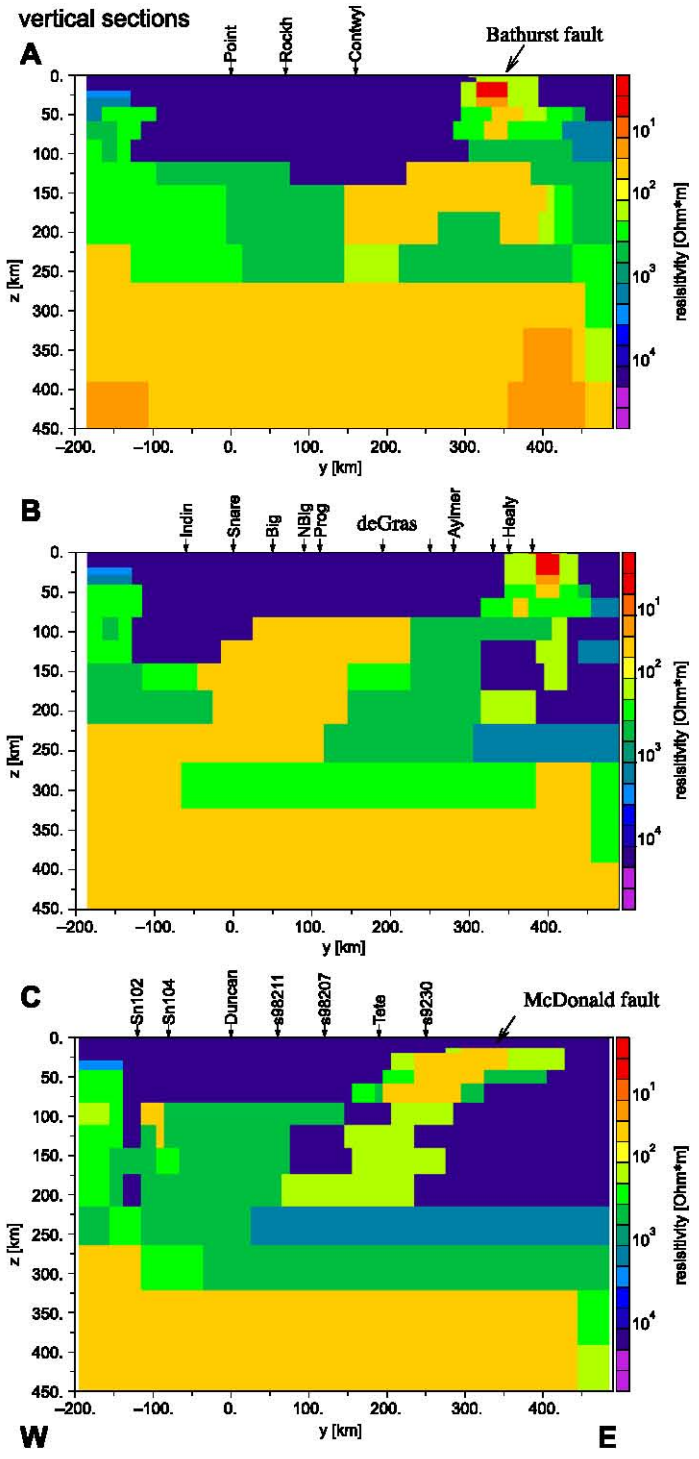

Fig. 9. Vertical slices through the 3-D model along profiles A, B, and C in Fig. 8.

react at longer periods than do the MT data for the same anomaly.) Three vertical E–W slices through the model, corresponding to profiles A, B, and C in Fig. 8, are shown in Fig. 9. Not shown are the comparison plots for other periods that were used during the forward trial-and-error model fitting exercise, which were 120, 320, 1200 and 2500 s.

The interpretations of 2-D modelling of the MT data from the winter road sites discussed previously demonstrate that the existence of a high conductivity zone encountered at depths of 80–120 km beneath the central Slave craton coincides spatially with the ultra-depleted harzburgitic layer in the upper mantle. The 3-D model traces this conductor as a NE–SW oriented mantle structure, with its centre located beneath Big, Providence and Lac de Gras lakes at a likely depth range of 70–250 km. In the eastern craton, the model contains highly conductive crustal vertical sheets beneath the Bathurst fault and a deeper NW dipping structure beneath the McDonald fault, suggesting the presence of conducting material (likely either graphite or sulphides) within a deep dipping fault zone. These we associate with the Thelon–Talston orogen (Jones et al., 2001b), and the size of the effect observed on the easternmost sites is quantitatively similar to sites on the Hearne hinterland of the Trans–Hudson orogen in northern Canada (Jones et al., 1993). In the case of the Trans–Hudson orogen, the conductivity anomaly, the well-known North American Central Plains conductivity anomaly, was shown to be associated with pyrite sulphides (Jones et al., 1997), and the same might also be true in the Thelon–Talston orogen.

The model fits the magnetic transfer functions (see the induction arrows in the plan view of Fig. 8) best, especially at long periods. The fit to the MT phases is partly satisfactory at periods >1000 s (with average RMS between 2 and 5). Two variations of the model structure below 230 km have been tested by setting a homogeneous half space of 50 and 500 Ω m below this depth, respectively. A superior fit to the data is found for the model with the 50 Ω m resistivity block at depth than with the 500 Ω m block, suggesting that the mantle below ~230 km depth cannot be resistive. This is consistent with the 1-D analyses presented above for the averaged Slave response. The responses of the 50 Ω m block model have a comparable data fit with that from the model shown here, hence indicating that the deep conductivity variations traced in the latter may or may not be necessary.

7. Discussion

7.1. Correlation with geochemical zones and Eocene kimberlites

The Central Slave Mantle Conductor corresponds spatially with two other observations from the Slave. As discussed in Jones et al. (2001a), it correlates with the location of a unique, two-layered lithospheric mantle in the central Slave craton extending over >9000 km^2 mapped by Griffin et al. (1999a,b). This layering comprises an ultra-depleted, harzburgitic upper layer (top undefined but shallower than ~100 km) separated sharply at 140–150 km depth (approx. graphite–diamond stability field) from a less depleted, lherzolitic lower layer.

When comparing those MT sites that are deemed to be on the CSMC, based on 2-D and 3-D modelling, with the NE–SW geochemical boundaries defined by Grütter et al. (1999) on the basis of garnet geochemistry (specifically G10 garnet populations), the spatial coincidence is remarkable (Fig. 6). With the sole exception of the lake bottom site BIG, all MT sites within Grütter's central zone are on the conductor, and all those outside that zone, either to the north or to the south, are off the conductor. This spatial association is explored further in Davis et al. (2003), where a tectonic history is developed for the Slave craton based, in part, on the geometry of the conductivity anomaly and its association with the garnet distributions.

Also remarkable is the close spatial association between the CSMC and the Eocene-aged kimberlite magmatism in the centre of the craton. The easternmost known Eocene kimberlite is on the western side of the northern arm of Aylmer Lake, in the middle of Profile 3. The 2-D model for that profile (Fig. 7D) shows that the mantle conductor ends precisely at that location.

7.2. Causes of conductivity enhancement

Olivine, orthopyroxene or clinopyroxene-dominated mineralogy would result in electrical resistivities in

excess of 100,000 Ω m in the SCLM at likely temperatures of hundreds to a thousand Celcius (Constable and Duba, 1990; Xu et al., 2000). In Jones et al. (2001a), various mechanisms were explored as possible candidates to explain the existence of the Central Slave Mantle Conductor. Two were proposed as favoured; carbon, either as grain-boundary films or as graphite, and diffusion of hydrogen. Others, such as partial melts, sulphides, saline fluids, hydrous mantle minerals, were all rejected. Partial melt we reject because there is no evidence for lithospheric delamination in the central Slave since the Eocene, when the lithosphere was 190 km thick based on petrological analyses of mantle xenoliths (Pearson et al., 1999). With regard to sulphides, for the Kaapvaal craton one could appeal to interconnected sulphides as the cause of enhanced conductivity, due to the observations of interstitial sulphides at the 330 ppm level (Alard et al., 2000); however, there is no evidence for sulphides in mantle xenoliths from the Slave craton (H. Grütter, pers. comm., 2001; B. Doyle, pers. comm., 2001; J. Gurney, pers. comm., 2001). Interconnected saline fluids we reject because of the age of the anomaly: the fluids are gravitationally unstable over geological time scales. Finally, hydrous mantle minerals, such as phlogopite (Boerner et al., 1999), we reject because when observed they are not interconnected, and metasomatism does not appear to be an agent that reduces resistivity (Jones et al., 2002). Also, hydrous crustal minerals do not enhance conductivity in the continental lower crust (Olhoeft, 1981).

The lake bottom data from the Lac de Gras station (Fig. 4) provide invaluable information that suggests the carbon interpretation is correct. First, the internal resistivity of the CSMC appears to be around 10–15 Ω m, which is too low for hydrogen diffusion at such shallow mantle depths (G. Hirth, 2001, pers. comm.). Second, the resistivity increases below the CSMC by a factor of 3–5 to 50 Ω m, consistent with graphite no longer being the dominant conductivity enhancement: the transition from carbon in conducting graphite form above the graphite–diamond stability field to carbon in highly resistive diamond form below the stability field occurs at 130 km (Griffin et al., 1999a). Craven and Jones (2001) demonstrated that the CSMC has a twin in the North Caribou terrane of the western part of the Superior Province, and suggest an environment for the reduction of carbon at upper mantle depths. Below the graphite–diamond stability field, the resistivity is still orders of magnitude less than an Ol–Cpx–Opx mineralogy would suggest, and possibly hydrogen diffusion (Karato, 1990) may be the valid explanation at these depths.

7.3. Tectonic implications

Griffin et al. (1999a,b) proposed that the unique two-layer petrological lithosphere comprising an upper SCLM harzburgite layer, from about 80–100 to about 140 km, underlain by a lower SCLM lherzolitic layer, was caused by trapped oceanic or arc-related lithosphere associated with the suturing of the western Slave craton to the eastern arc terrane, now dated at ca. 2690 Ma (Davis and Bleeker, 1999). This ultra-depleted lithosphere is thought to have been subsequently underlain by plume lithosphere to explain ultra-deep ferropericlase and Mg-perovskite diamonds (Davies et al., 1999).

We have demonstrated that the Central Slave Mantle Conductor is intimately spatially associated with this ultra-depleted layer, which suggests an ancient provenance for the CSMC. However, the geometry of the CSMC has a NE–SW strike and a NW dip, inconsistent with E–W convergence. Although oblique convergence could have occurred, the spatial orientation of the anomaly with the later post-accretion deformation and plutonism is taken as firm evidence of an association with later tectonism (see Davis et al., 2003). Taken together with other petrological, geochemical and geophysical information from the Slave's SCLM, we conclude that the CSMC is a consequence of subcretion at ca. 2630 Ma by exotic lithosphere from the SE. This is discussed further in Davis et al. (2003).

8. Conclusions

Deep-probing electromagnetic studies, using the magnetotelluric (MT) technique, are capable of contributing significantly to the understanding of the formation and evolution of Archean lithosphere. Herein, we show that such studies on the Slave craton have imaged serendipitously a remarkable anomaly in electrical conductivity located within the upper part of the sub-continental lithospheric mantle in the centre of the

craton. This anomaly, named the Central Slave Mantle Conductor (CSMC), correlates with geochemical information obtained from mantle xenoliths and with the known exposures of Eocene-aged kimberlites. Given the internal resistivity of the conductor, 10–15 Ω m, given its limited depth extent to the graphite–diamond stability field, and given the various plausible candidates for explaining enhanced conductivity, we conclude that the anomaly is due to carbon as either graphite or as carbon on grain-boundary films.

We ascribe a Neoarchean age to the CSMC, given the spatial correlation with Griffin et al.'s (1999a,b) harzburgitic ultra-depleted layer and with the occurrence of G10 garnets mapped by Grütter et al. (1999), and suggest that it was emplaced as a consequence of sub-cretion by exotic lithosphere from the SE at ca. 2630–2590 Ma. The spatial association with the Eocene kimberlite magmatism is intriguing, and we speculate that the rheological differences between the different mantle domains may have influenced where the kimberlties were able to erupt.

Features in the northern part of the craton we are less certain about, given the paucity of MT sites. We intend to rectify this with deep-probing MT measurements over the next few years.

Acknowledgements

The electromagnetic experiments on the Slave craton were made possible through the financial support and logistical efforts of many organizations, companies and individuals. Financial support came from LITHOPROBE, Geological Survey of Canada (GSC, under the LITHOPROBE, EXTECH-III and Walmsley Lake Targeted Geoscience Initiative programs), Canadian Federal Department of Indian and Northern Development (DIAND), the U.S. National Science Foundation's Continental Dynamics Program, DeBeers Canada Exploration, Kennecott Exploration and BHP Billiton Diamonds Logistical support was provided by Diavik, BHP Billiton, DeBeers and Winspear, and in Yellowknife by Royal Oak Mines and Miramar Mining. Data acquisition along the all-weather and winter roads in 1996, 1998 and 1999 was undertaken by Phoenix Geophysics, and in 2000 by Geosystem Canada, who are thanked for their support in terms of reduced academic survey rates and close attention to detail which resulted in high quality responses. The staff of the Yellowknife Seismological Observatory is thanked for its support and for providing essential preparation facilities. The lake bottom sites were deployed and retrieved from a Twin Otter float plane with a specially designed winch built for us by Air Tindi. Finally, we wish to thank all our colleagues for enlightening discussions. Particular individuals whom we wish to recognise as contributing to our efforts include Alex Arychuk (Air Tindi), Wouter Bleeker (GSC), Bill Davis (GSC), Buddy Doyle (Kennecott Exploration), Garth Eggenberger (Air Tindi), Leo Fox (Phoenix), Nick Grant (formerly GSC, now University of Victoria), Herman Grütter (formerly DeBeers Canada Exploration, now Mineral Services Canada), Colin Farquharson (UBC), George Jensen (Yellowknife GSC), Leonard Johnson (NSF), Andy Langlois (formerly Yellowknife GSC), Juanjo Ledo (formerly GSC, now University of Barcelona), Grant Lockhart (BHP Billiton Diamonds), Gary McNeice (formerly Phoenix Geophysics, now Geosystem Canada), Brian Roberts (GSC), David Snyder (GSC), and Carolyn Relf (DIAND), and, most especially, Hendrik Falck (C.S. Lord Northern Geoscience Centre).

The data were modelled using 2-D and 3-D codes within the Geotools program, with updates from Randy Mackie. The data were contoured using Paul Wessel's GMT package.

Geological Survey of Canada Contribution No. 2002002. Lithoprobe publication No. 1339. Woods Hole Oceanographic Institution Contribution 11023.

References

Alard, O., Griffin, W.L., Lorand, J.P., Jackson, S.E., O'Reilly, S.Y., 2000. Non-chondritic distribution of the highly siderophile elements in mantle sulphides. Nature 407, 891–894.

Ashwal, L.D., Burke, K., 1989. African lithospheric structure, volcanism, and topography. Earth Planet. Sci. Lett. 96, 8–14.

Bailey, R.C., 1970. Inversion of the geomagnetic induction problem. Proc. R. Soc. Lond., A 315, 185–194.

Bank, C.-G., Bostock, M.G., Ellis, R.M., Cassidy, J.F., 2000. A reconnaissance teleseismic study of the upper mantle and transition zone beneath the Archean Slave craton in NW Canada. Tectonophysics 319, 151–166.

Bendat, J.S., Piersol, A.G., 1971. Random Data: Analysis and Measurement Procedures. Wiley-Interscience, New York.

Bentley, C.R., 1973. Error estimation in two dimensional magnetotelluric analyses. Phys. Earth Planet. Inter. 7, 423–430.

Berdichevsky, M.N., Dmitriev, V.I., 1976. Basic principles of interpretation of magnetotelluric sounding curves. In: Adam, A. (Ed.), Geoelectric and Geothermal Studies. KAPG Geophysical Monograph, Akademiai Kiad, pp. 165–221.

Bleeker, W., Davis, W.J., 1999. The 1991–1996 NATMAP slave province project: introduction. Can. J. Earth Sci. 36, 1033–1042.

Bleeker, W., Ketchum, J.W.F., Jackson, V.A., Villeneuve, M.E., 1999a. The Central Slave Basement Complex: Part I. Its structural topology and autochthonous cover. Can. J. Earth Sci. 36, 1083–1109.

Bleeker, W., Ketchum, J.W.F., Davis, W.J., 1999b. The Central Slave Basement Complex: Part II. Age and tectonic significance of high-strain zones along the basement–cover contact. Can. J. Earth Sci. 36, 1111–1130.

Boerner, D.E., Kurtz, R.D., Craven, J.A., Ross, G.M., Jones, F.W., Davis, W.J., 1999. Electrical conductivity in the Precambrian lithosphere of Western Canada. Science 283, 668–670.

Bostock, M.G., 1998. Mantle stratigraphy and evolution of the Slave province. J. Geophys. Res. 103, 21183–21200.

Bostock, M.G., Cassidy, J.F., 1997. Upper mantle stratigraphy beneath the southern Slave Craton. Can. J. Earth Sci. 34, 577–587.

Carbno, G.B., Canil, D., 2002. Mantle structure beneath the SW Slave Craton, Canada; constraints from garnet geochemistry in the Drybones Bay Kimberlite. J. Petrol. 43, 129–142.

Cavaliere, T., Jones, A.G., 1984. On the identification of a transition zone in electrical conductivity between the lithosphere and asthenosphere: a plea for more precise phase data. J. Geophys. 55, 23–30.

Chave, A.D., Thomson, D.J., 2003. A bounded influence regression estimator based on the statistics of the hat matrix. J. Roy. Stat. Soc. Series C, Appl. Stat. 52, 307–322.

Constable, S.C., Duba, A., 1990. Electrical conductivity of olivine, a dunite, and the mantle. J. Geophys. Res. 95, 6967–6978.

Constable, S.C., Parker, R.L., Constable, C.G., 1987. Occam's inversion: a practical algorithm for generating smooth models from electromagnetic sounding data. Geophysics 52, 289–300.

Cook, F.A., van der Velden, A.J., Hall, K.W., Roberts, B.J., 1999. Frozen subduction in Canada's Northwest Territories; lithoprobe deep lithospheric reflection profiling of the western Canadian Shield. Tectonics 18, 1–24.

Cookenboo, H.O., 1999. History and process of emplacement of the Jericho (JD-1) kimberlite pipe, northern Canada. In: Gurney, J.J., Gurney, J.L., Pascoe, M.D., Richardson, S.H. (Eds.), The J.B. Dawson Volume; Proceedings of the VIIth International Kimberlite Conference; Volume 1. Proceedings of the International Kimberlite Conference. 7, vol. 1, pp. 125–133.

Craven, J.A., Jones, A.G, 2001. Comparison of Slave and Superior electrical lithospheres. Presented at the Slave-Kaapvaal Workshop, Merrickville, Ontario, Canada, September 2001.

Davies, R.M., Griffin, W.L., Pearson, N.J., Andrew, A.S., Doyle, B.J., O'Reilly, S.Y., 1999. Diamonds fron the deep: Pipe DO-27, Slave craton, Canada. The 7th International Kimberlite Conference Proceedings. J.B. Dawson Volume, vol. 1, pp. 148–155.

Davis, W.J., Bleeker, W., 1999. Timing of plutonism, deformation, and metamorphism in the Yellowknife Domain, Slave Province, Canada. Can. J. Earth Sci. 36, 1169–1187.

Davis, W.J., Hegner, E., 1992. Neodymium isotopic evidence for the accretionary development of the Late Archean Slave Province. Contrib. Mineral. Petrol. V. 111, 493–504.

Davis, W.J., Gariepy, C., van Breeman, O., 1996. Pb isotopic composition of late Archean granites and the extent of recycling early Archean crust in the Slave Province, northwest Canada. Chem. Geol. 130, 255–269.

Davis, W.J., Jones, A.G., Bleeker, W., Grütter, H., 2003. Lithospheric development in the Slave Craton: a linked crustal and mantle perspective. Lithos 71, 575–589 (this issue).

Drury, M.R., Fitz Gerald, J.D., 1996. Grain boundary melt films in an experimentally deformed olivine–orthopyroxene rock; implications for melt distribution in upper mantle rocks. Geophys. Res. Lett. 23, 701–704.

Edwards, R.N., Bailey, R.C., Garland, G.D., 1981. Conductivity anomalies: lower crust or asthenosphere? Phys. Earth Planet. Inter. 25, 263–272.

Fipke, C.E., Dummett, H.T., Moore, R.O., Carlson, J.A., Ashley, R.M., Gurney, J.J., Kirkley, M.B., 1995. History of the discovery of diamondiferous kimberlites in the Northwest Territories, Canada. Sixth International Kimberlite Conference; Extended Abstracts. Proceedings of the International Kimberlite Conference, vol. 6, pp. 158–160.

Fischer, G., Le Quang, B.V., 1981. Topography and minimization of the standard deviation in one-dimensional magnetotelluric modelling. Geophys. J. R. Astron. Soc. 67, 279–292.

Fischer, G., Schnegg, P.-A., Peguiron, M., Le Quang, B.V., 1981. An analytic one-dimensional magnetotelluric inversion scheme. Geophys. J. R. Astron. Soc. 67, 257–278.

Garcia, X., Jones, A.G., 2000. Regional scale survey of the Yellowknife fault. Contributed paper at: Yellowknife Geoscience Forum, Yellowknife, NWT, 22–24 November.

Garcia, X., Chave, A.D., Jones, A.G., 1997. Robust processing of magnetotelluric data from the auroral zone. J. Geomagn. Geoelectr. 49, 1451–1468.

Griffin, W.L., Doyle, B.J., Ryan, C.G., Pearson, N.J., O'Reilly, S.Y., Davies, R., Kivi, K., van Achterbergh, E., Natapov, L.M., 1999a. Layered mantle lithosphere in the Lac de Gras area, Slave craton: composition, structure and origin. J. Petrol. 40, 705–727.

Griffin, W.L., Doyle, B.J., Ryan, C.G., Pearson, N.J., O'Reilly, S.Y., Natapov, L., Kivi, K., Kretschmar, R., Ward, J., 1999b. Lithosphere structure and mantle terranes: Slave Craton, Canada. The 7th International Kimberlite Conference Proceeding. J.B. Dawson Volume, vol. 1, pp. 299–306.

Grütter, H.S., Apter, D.B., Kong, J., 1999. Crust–mantle coupling; evidence from mantle-derived xenocrystic garnets. Contributed paper at the 7th International Kimberlite Conference Proceeding. J.B. Dawson Volume, vol. 1, pp. 307–313.

Heaman, L.M., Creaser, R.A., Cookenboo, H.O., 2002. Extreme enrichment of high field strength elements in Jericho eclogite xenoliths; a cryptic record of Paleoproterozoic subduction, par-

tial melting, and metasomatism beneath the Slave Craton, Canada. Geology 30, 507–510.

Helmstaedt, H.H., Schulze, D.J., 1989. Southern African kimberlites and their mantle sample: implications for Archean tectonics and lithosphere evolution. In: Ross, J. (Ed.), Kimberlites and Related Rocks, vol. 1: Their Composition, Occurrence, Origin, and Emplacement. Geological Society of Australia Special Publication, vol. 14, pp. 358–368.

Hirth, G., Evans, R.L., Chave, A.D., 2000. Comparison of continental and oceanic mantle electrical conductivity: is the Archean lithosphere dry? Geochem. Geophys. Geosyst. 1, paper number 2000GC000048.

Hoffman, P., 1988. United plates of America, the birth of a craton: early Proterozoic assembly and growth of Proto–Laurentia. Annu. Rev. Earth Planet. Sci. 16, 543–603.

Jones, A.G., 1982. On the electrical crust–mantle structure in Fennoscandia: no Moho and the asthenosphere revealed? Geophys. J. R. Astron. Soc. 68, 371–388.

Jones, A.G., 1986. Parkinson's pointers' potential perfidy! Geophys. J. R. Astron. Soc. 87, 1215–1224.

Jones, A.G., 1988. Static shift of magnetotelluric data and its removal in a sedimentary basin environment. Geophysics 53, 967–978.

Jones, A.G., 1992. Electrical conductivity of the continental lower crust. In: Fountain, D.M., Arculus, R.J., Kay, R.W. (Eds.), Continental Lower Crust. Elsevier, Amsterdam, pp. 81–143. Chap. 3.

Jones, A.G., 1993. Electromagnetic images of modern and ancient subduction zones. In: Green, A.G., Kroner, A., Gotze, H.-J., Pavlenkova, N. (Eds.), Plate Tectonic Signatures in the Continental Lithosphere. Tectonophysics, vol. 219, pp. 29–45.

Jones, A.G., 1998. Waves of the future: superior inferences from collocated seismic and electromagnetic experiments. Tectonophysics 286, 273–298.

Jones, A.G., 1999. Imaging the continental upper mantle using electromagnetic methods. Lithos 48, 57–80.

Jones, A.G., Ferguson, I.J., 2001. The electric Moho. Nature 409, 331–333.

Jones, A.G., Jödicke, H., 1984. Magnetotelluric transfer function estimation improvement by a coherence-based rejection technique. Contributed paper at 54th Society of Exploration Geophysics Annual General Meeting. Atlanta, Georgia, U.S.A., December 2–6, pp. 51–55. Abstract volume.

Jones, A.G., Spratt, J., 2002. A simple method for deriving the uniform field MT responses in auroral zones. Earth Planets Space 54, 443–450.

Jones, A.G., Chave, A.D., Egbert, G., Auld, D., Bahr, K., 1989. A comparison of techniques for magnetotelluric response function estimation. J. Geophys. Res. 94, 14201–14213.

Jones, A.G., Craven, J.A., McNeice, G.A., Ferguson, I.J., Boyce, T., Farquharson, C., Ellis, R.G., 1993. The North American Central Plains conductivity anomaly within the Trans–Hudson orogen in northern Saskatchewan. Geology 21, 1027–1030.

Jones, A.G., Katsube, J., Schwann, P., 1997. The longest conductivity anomaly in the world explained: sulphides in fold hinges causing very high electrical anisotropy. J. Geomagn. Geoelectr. 49, 1619–1629.

Jones, A.G., Ferguson, I.J., Chave, A.D., Evans, R.L., McNeice, G.W., 2001a. The electric lithosphere of the Slave craton. Geology 29, 423–426.

Jones, A.G., Snyder, D., Spratt, J., 2001b. Magnetotelluric and teleseismic experiments as part of the Walmsley Lake project: experimental designs and preliminary results. Geol. Surv. Can. Curr. Res. C6, 10-1–10-4.

Jones, A.G., Snyder, D., Hanmer, S., Asudeh, I., White, D., Eaton, D., Clarke, G., 2002. Magnetotelluric and teleseismic study across the Snowbird Tectonic Zone, Canadian Shield: a Neoarchean mantle suture? Geophys. Res. Lett. 29 (10), 10-1–10-4 doi: 10.1029/2002GL015359.

Jordan, T.H., 1988. Structure and formation of the continental tectosphere. J. Petrol., Special Lithosphere Issue, 11–37.

Karato, S., 1990. The role of hydrogen in the electrical conductivity of the upper mantle. Nature 347, 272–273.

Kopylova, M.G., 2002. The deep structures of the Slave Craton. Presented at "Diamond Short Course", held in Vancouver, Canada, B.C., 21 February.

Kopylova, M.G., Russel, J.K., Cookenboo, H., 1997. Petrology of peridotite and pyroxenite xenoliths from Jericho Kimberlite; implications for the thermal state of the mantle beneath the Slave Craton, northern Canada. J. Petrol. 40, 79–104.

Kurtz, R.D., Craven, J.A., Niblett, E.R., Stevens, R.A., 1993. The conductivity of the crust and mantle beneath the Kapuskasing Uplift: electrical anisotropy in the upper mantle. Geophys. J. Int. 113, 483–498.

Kusky, T.M., 1989. Accretion of the Archean Slave province. Geology 17, 63–67.

Kusky, T.M., Polet, A., 1999. Growth of granite–greenstone terranes at convergent margins, and stabilization of Archean cratons. Tectonophysics 305, 43–73.

Lezaeta, P., Haak, V., 2003. Beyond MT decomposition: Induction, current channeling and magnetotelluric phases over 90°. J. Geophys. Res. 108 (B6), 2305. doi:10.1029/2001JB000990

MacKenzie, J.M., Canil, D., 1999. Composition and thermal evolution of cratonic mantle beneath the central Archean Slave Province, NWT, Canada. Contrib. Mineral. Petrol. 134, 313–324.

Mackie, R.L., Madden, T.R., 1993. Conjugate direction relaxation solutions for 3-D magnetotelluric modeling. Geophysics 58, 1052–1057.

Mackie, R.L., Madden, T.R., Wannamaker, P.E., 1993. Three-dimensional magnetotelluric modeling using difference equations; theory and comparisons to integral equation solutions. Geophysics 58, 215–226.

Mackie, R.L., Smith, J.T., Madden, T.R., 1994. Three-dimensional electromagnetic modeling using finite difference equations: the magnetotelluric example. Radio Sci. 29, 923–935.

McNeice, G.W., Jones, A.G., 1998. Magnetotellurics in the frozen north: measurements on lake ice. Contributed paper at 14th EM Induction Workshop, Sinaia, Romania, August 16–23.

Minarik, W.G., Watson, E.B., 1995. Interconnectivity of carbonate melt at low melt fraction. Earth Planet. Sci. Lett. 133, 423–437.

Nakano, T., Fujii, N., 1989. The multiphase grain control percolation; its implication for a partially molten rock. J. Geophys. Res. 94, 15653–15661.

Olhoeft, G.R., 1981. Electrical properties of granite with implications for the lower crust. J. Geophys. Res. 86, 931–936.

Padgham, W.A., Fyson, W.K., 1992. The Slave Province: a distinct Archean craton. Can. J. Earth Sci. 29, 2072–2086.

Parker, R.L., 1980. The inverse problem of electromagnetic induction: existence and construction of solutions based on incomplete data. J. Geophys. Res. 85, 4421–4425.

Parker, R.L., Booker, J.R., 1996. Optimal one-dimensional inversion and bounding of magnetotelluric apparent resistivity and phase measurements. Phys. Earth Planet. Inter. 98, 269–282.

Parker, R.L., Whaler, K.A., 1981. Numerical methods for establishing solutions to the inverse problem of electromagnetic induction. J. Geophys. Res. 86, 9574–9584.

Parkinson, W.D., 1962. The influence of continents and oceans on geomagnetic variations. Geophys. J. R. Astron. Soc. 6, 441–449.

Partzsch, G.M., Schilling, F.R., Arndt, J., 2000. The influence of partial melting on the electrical behavior of crustal rocks: laboratory examinations, model calculations and geological interpretations. Tectonophysics 317, 189–203.

Pearson, N.J., Griffin, W.L., Doyle, B.J., O'Reilly, S.Y., Van Achterbergh, E., Kivi, K., 1999. Xenoliths from kimberlite pipes of the Lac de Gras area, Slave craton, Canada. In: Gurney, J.J., et al. (Eds.), Proceedings of the 7th international Kimberlite conference. P.H. Nixon, vol. 2. Red Roof Design, Cape Town, pp. 644–658.

Petitt Jr., R.A., Chave, A.D., Filloux, J.H., Moeller, H.H., 1994. Electromagnetic field instrument for the continental shelf. Sea Technol. 35, 10–13.

Rodi, W., Mackie, R.L., 2001. Nonlinear conjugate gradients algorithm for 2-D magnetotelluric inversion, in press. Geophysics 66, 174–187.

Schilling, F.R., Partzsch, G.M., Brasse, H., Schwarz, G., 1997. Partial melting below the magmatic arc in the central Andes deduced from geoelectromagnetic field experiments and laboratory data. Phys. Earth Planet. Inter. 103, 17–31.

Schmucker, U., 1970. Anomalies of geomagnetic variations in the southwestern United States. Bull. Scripps Inst. Oceanogr., vol. 13. Univ. Calif. Press, Berkeley.

Schultz, A., Kurtz, R.D., Chave, A.D., Jones, A.G., 1993. Conductivity discontinuities in the upper mantle beneath a stable craton. Geophys. Res. Lett. 20, 2941–2944.

Snyder, D., Asudeh, I., Darbyshire, F., Drysdale, J., 2002. Field-based feasibility study of teleseismic surveys at high northern latitudes: Northwest Territories and Nunavut. Geological Survey of Canada Current Research, 2002-C03. 10 pp.

Stern, R.A., Bleeker, W., 1998. Age of the world's oldest rocks refined using Canada's SHRIMP: the Acasta Gneiss Complex, Northwest Territories, Canada. Geosci. Can. 25, 27–31.

Sternberg, B.K., Washburne, J.C., Pellerin, L., 1988. Correction for the static shift in magnetotellurics using transient electromagnetic soundings. Geophysics 53, 1459–1468.

Thompson, P.H., Judge, A.S., Lewis, T.J., 1996. Thermal evolution of the lithosphere in the central Slave Province: implications for diamond genesis. In: LeCheminant, A.N., Richardson, D.G., DiLabio, R.N.W., Richardson, K.A. (Eds.), Searching for Diamonds in Canada. Geol. Surv. Canada, pp. 151–160. Open File 3228.

Thorpe, R.I., Cumming, G.L., Mortensen, J.K., 1992. A significant Pb isotope boundary in the Slave Province and its probable relation to ancient basement in the western Slave Province. Project Summaries, Canada-Northwest Territories mineral Development Subsidiary Agreement. Geol. Surv. Canada, pp. 279–284. Open-File Report 2484.

Tikhonov, A.N., Glasko, V.B., 1975. Application of the regularization method to geophysical interpretation problems. Phys. Solid Earth 11, 25–32.

Viejo, G.F., Clowes, R.M., Amor, J.R., 1999. Imaging the lithospheric mantle in northwestern Canada with seismic wide-angle reflections. Geophys. Res. Lett. 26, 2809–2812.

Vozoff, K. (Ed.), 1986. Magnetotelluric Methods. Soc. Expl. Geophys. Reprint Ser., vol. 5. Tulsa, OK, ISBN 0-931830-36-2.

Vozoff, K., 1991. The magnetotelluric method. Electromagnetic Methods in Applied Geophysics—Applications. Society of Exploration Geophysicists, Tulsa, OK, pp. 641–712. Chap. 8.

Weidelt, P., 1972. The inverse problem of geomagnetic induction. Z. Geophys. 38, 257–289.

Wessel, P., Smith, W.H.F., 1991. Free software help map and display data. EOS 72, 441.

Wu, X., Ferguson, I.J., Jones, A.G., 2002. Magnetotelluric response and geoelectric structure of the Great Slave Lake shear zone. Earth Planet. Sci. Lett. 196, 35–50.

Xu, Y., Shankland, T.J., Poe, B.T., 2000. Laboratory-based electrical conductivity of the Earth's mantle. J. Geophys. Res. 105, 27865–27875.